

Chapter 4

BEAM OPTICS OF SESAME IV

4.1 Introduction

The lattice flexibility is an important issue for the synchrotron light source. In SESAME III proposal (that in the yellow book), pole face windings were suggested to have some vertical focusing flexibility. It has been seen that the pole face windings provide a limited flexibility in addition to the fact that their installation could be difficult and not guaranteed.

So, a new lattice has been proposed in order to avoid the risk of the pole face windings. The new proposal is called SESAME IV.

4.2 The Lattice

4.2.1 The Unit Cell

To recover the vertical flexibility, the pole face windings were cancelled and replaced by a normal defocusing magnet.

Due to the high need to space between elements, the field flux was increased from 1.4T to 1.425T which resulted in decreasing the curvature radius from 5.9565 to 5.85201m. The new length of the bending magnet became 2.3m and the old quadrupoles and spaces have been shortened a little bit. The net change on the ring circumference was the increase from 124.8m to 128.2m.

The gradient in the bending has been reduced from -3.032T/m to -2.377T/m .

The upgraded SESAME lattice is shown in figure (4.1), and its structure elements are given by table (4.1)

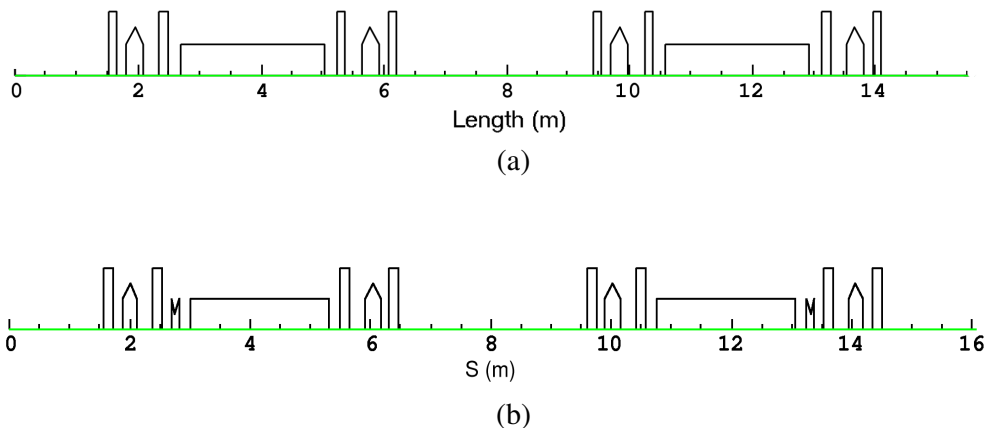


Figure 4.1: The structure of one super period (2cells) of: (a) the yellow book lattice and (b) the upgraded lattice.

SESAME IV optical functions are shown in figure (4.2) while SESAME storage ring parameters are given in table (4.2).

Table 4.1: The lattice elements of half-super period structure.
The total ring is 8 super periods.

Name code	Element	Length (m)	ρ (m)	k (m^{-2})	m (m^{-3})
1	D1	1.575			
2	S1	.14			5.9724
3	D2	.155			
4	Q1	.26		2.2534	
5	D3	.255			
6	S2	.14			-8.2598
7	D4	.165			
8	Q2	.11		-2.0589	
9	D5	.2			
10	BM	2.298	5.852	-2.377	
11	D6	.205			
12	S3	.14			-17.0211
13	D7	.255			
14	Q3	.26		2.2166	
15	D8	.155			
16	S4	.14			12.2909
17	D8	1.575			

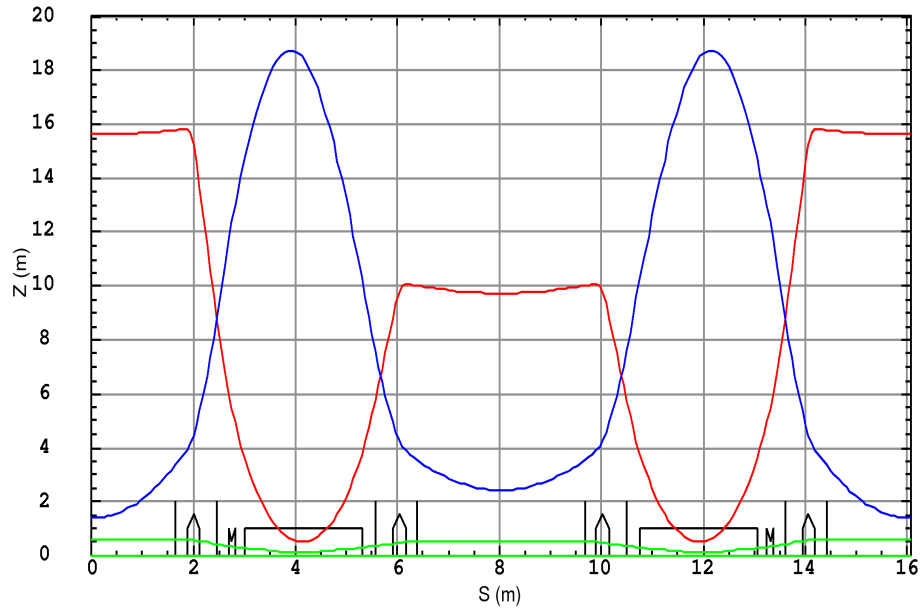


Figure 4.2: Optical functions of SESAME IV lattice. β_x and β_z and dispersion are represented by red, blue and green lines respectively.

**Table 4.2: SESAME storage ring parameters
(without insertion devices).**

Parameter	Unit	Value
General Parameters		
Energy	GeV	2.5
Maximum Beam current	mA	400
Circumference	m	128.2
Natural emittance	nm.rad	26.5
Coupling	%	1
Horizontal emittance	nm.rad	26.14
Vertical emittance	nm.rad	.265
Horizontal tune		7.23
Vertical tune		5.19
Relative energy spread	%	.104
Natural chromaticity (horizontal)		-14.62
Natural chromaticity (vertical)		-13.65
$\Sigma(\text{str. section length}) / \text{circumference}$	%	37.4
Machine Functions		
<i>Horizontal beta functions</i>		
Wiggler / bending / undulator	m/rad	15.6 / .495 / 9.72
<i>Vertical beta functions</i>		
Wiggler / bending / undulator	m/rad	1.37 / 18.72 / 2.41
<i>Dispersion function</i>		
Wiggler / bending / undulator	m	.56 / .131 / .478
Beam Sizes and Cross Sections		
<i>Horizontal beam size</i>		
Wiggler / bending / undulator	μm	864.3 / 176.7 / 709.4
<i>Vertical beam size</i>		
Wiggler / bending / undulator	μm	19 / 70.4 / 25.3
<i>Beam area</i>		
Wiggler / bending / undulator	mm^2	0.103 / 0.078 / 0.113
R.F-System		
Energy loss (bending)/ turn	keV	590.74
R.F-frequency	MHz	499.7
Harmonic number		214
R.F-power	kW	500
Number of cavities		4
Shunt impedance per cavity	$\text{M}\Omega$	8.583
Total cavity voltage	kV	2400
Over voltage factor		4
Energy acceptance	%	1.46
Bunch length	mm	11.13

4.2.2 The Working Point

The chosen working point is (7.23, 5.19) which is very close to the one of SESAME III and it was chosen due to the same reasons. So, the resonance lines around the working point and their level of gravity can be considered as in SESAME III case. Figure (4.3) shows the tune diagram of SESAME IV working point.

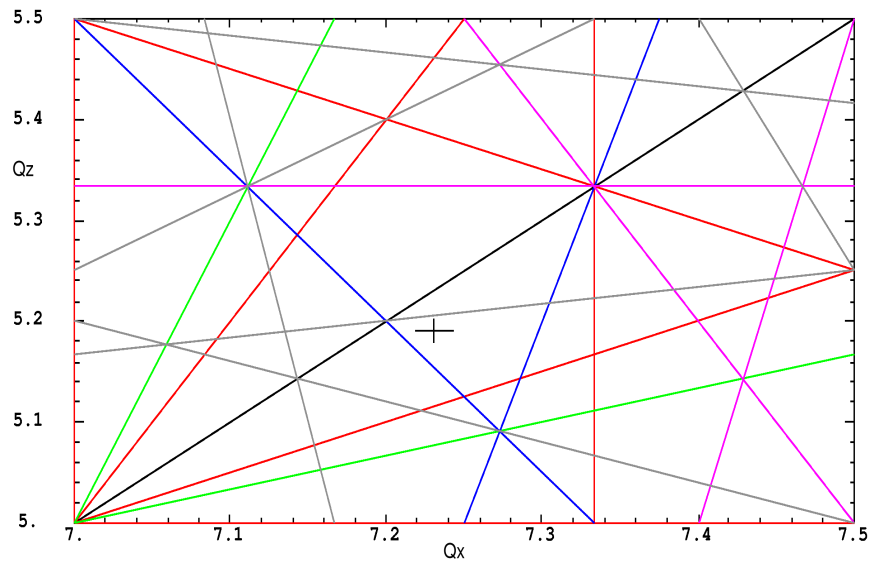


Figure 4.3: Tune diagram shows all the 2nd order (in black) and 3rd order (in red) resonance as well as the systematic 4th (in green), 5th (in blue), 6th (in pink) and 7th (in grey) order resonance.

4.2.3 The Tune Shift with Amplitude

The tune shifts with amplitude were kept as smooth as possible with a special care given to the horizontal one due to the fact that the large betatron excursions will be in the horizontal plane. This can be seen by figure (4.4) for a particle tracked over 700 turns.

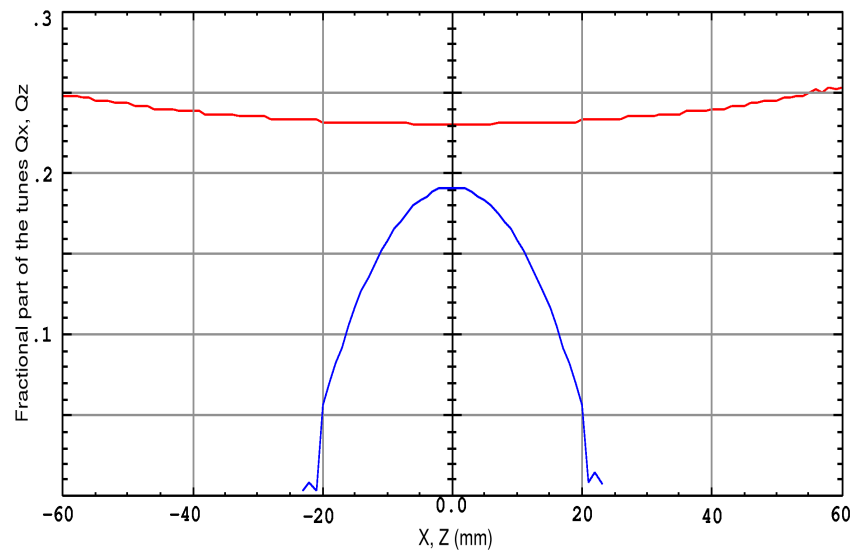


Figure 4.4: Tune shift with betatron amplitude with chromaticity = 2 in both planes. The horizontal (in red) tune is with integer part = 7 and the vertical one (in blue) is with integer part = 5.

4.2.4 The Dynamic Aperture

Figure (4.5) shows the dynamic aperture of SESAME IV. The limiting physical aperture is the same as in SESAME III. It should be noted that these calculations have been done at the beginning of the cell where $\beta_x = 15.6\text{m}$ and $\beta_z = 1.37\text{m}$.

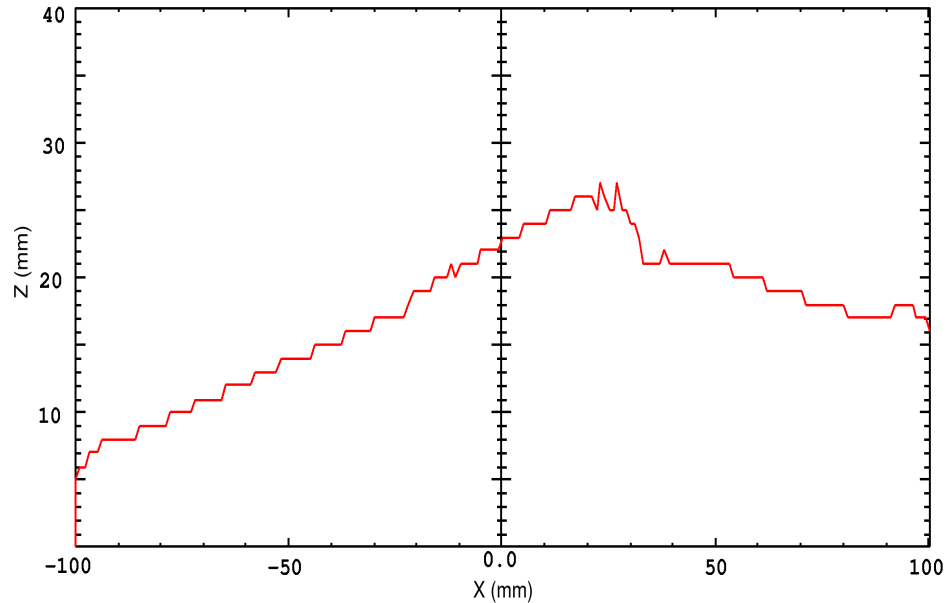


Figure 4.5: Dynamic aperture (in red) for on-momentum particle, calculated over 700 turns.

In comparison with the dynamic aperture of SESAME III taking into account the different values of the horizontal and vertical beta functions; we find it here better in the vertical plane than before.

Tracking the on-momentum particle horizontally and vertically at different locations will give more clear idea about the new beam dynamics. This can be shown by figures (4.6) and (4.7) respectively.

In figure (4.6) the particle has been tracked horizontally, at $Z = 1\text{E-}5\text{m}$, at each 5mm on the X-axis. It can be seen that an effect of non-linearities start to deform the shape of the ellipse at $x= 20\text{mm}$ and that the deformation becomes stronger at higher amplitudes but the particles still stable.

In figure (4.7) the particle has been tracked vertically, at $X= 1\text{e-}5\text{m}$, at each 2mm on the Z-axis. The ellipse deformation starts at $z =20\text{mm}$ keeping the particle stable.

This tracking shows the high beam stability taking into account that the tracking has been done at the beginning of the lattice where the needed physical half-apertures are 27.5mm horizontally and 4mm vertically.

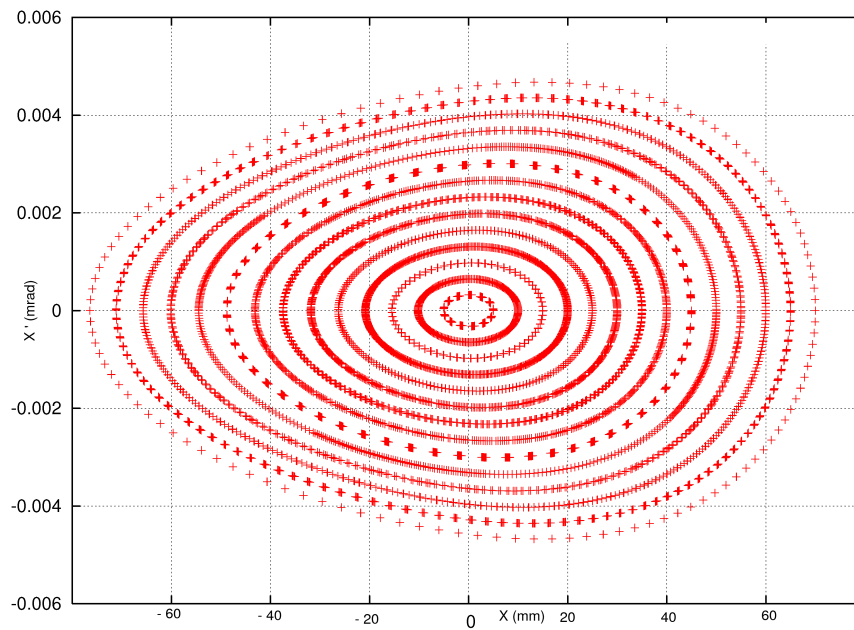


Figure 4.6: The horizontal phase space (at $z = 1e-5m$) of the on-momentum particle.

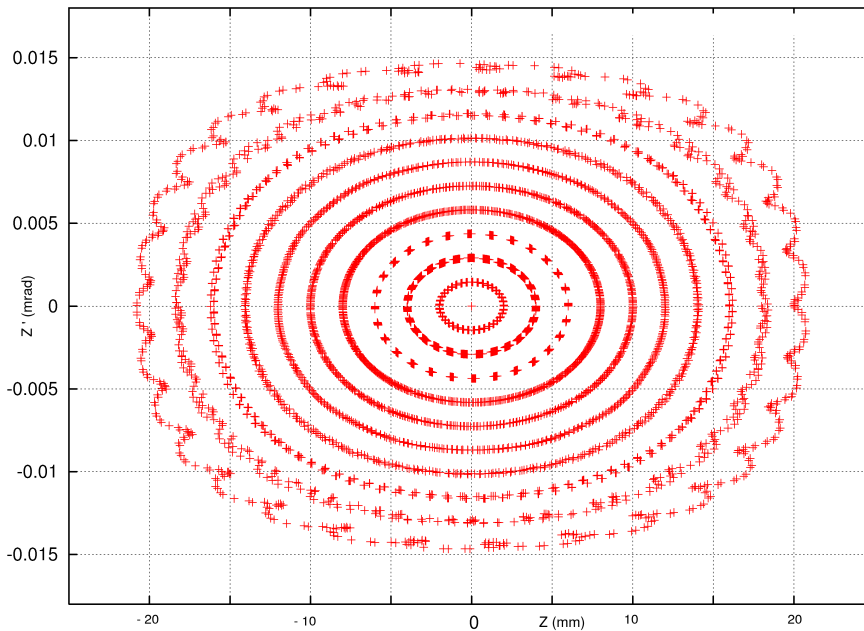


Figure 4.7: The vertical phase space (at $x = 1e-5m$) of the on-momentum particle.

4.2.5 The Off-momentum Dynamics

The tune shift with energy deviation is shown in figure (4.8). As can be seen from the graph, the horizontal tune crosses the 3rd order resonance (which may be destructive) after $dp/p = 3\%$ indicating to a good momentum aperture.

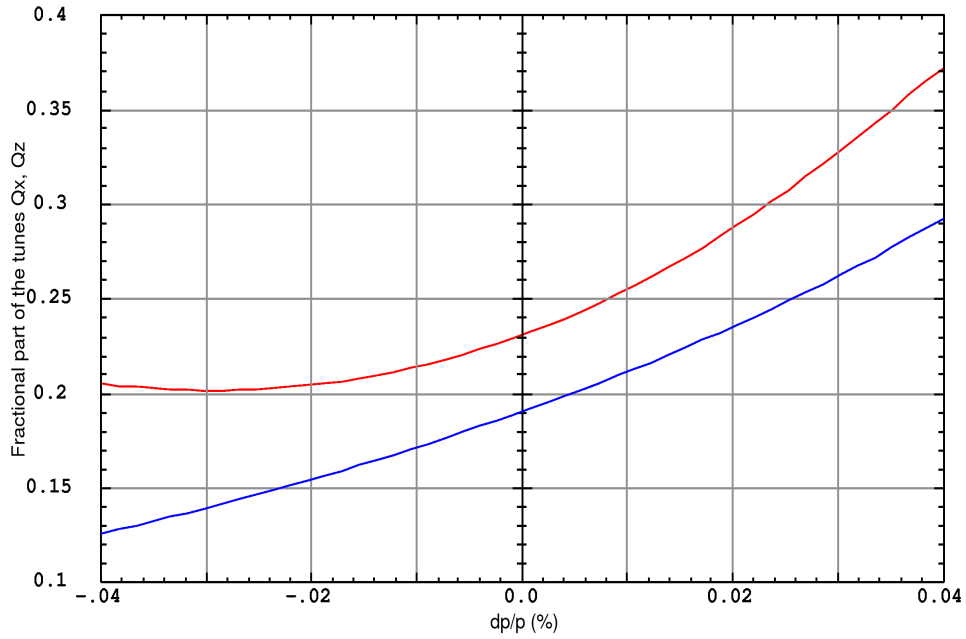


Figure 4.8: Horizontal (in red) and vertical (in blue) tune shifts with momentum deviation. Corrected chromaticity = 2 in both planes.

More details about the behaviour of the off-momentum particles are given by figure (4.9) which displays the horizontal tune shifts with amplitude for these particles.

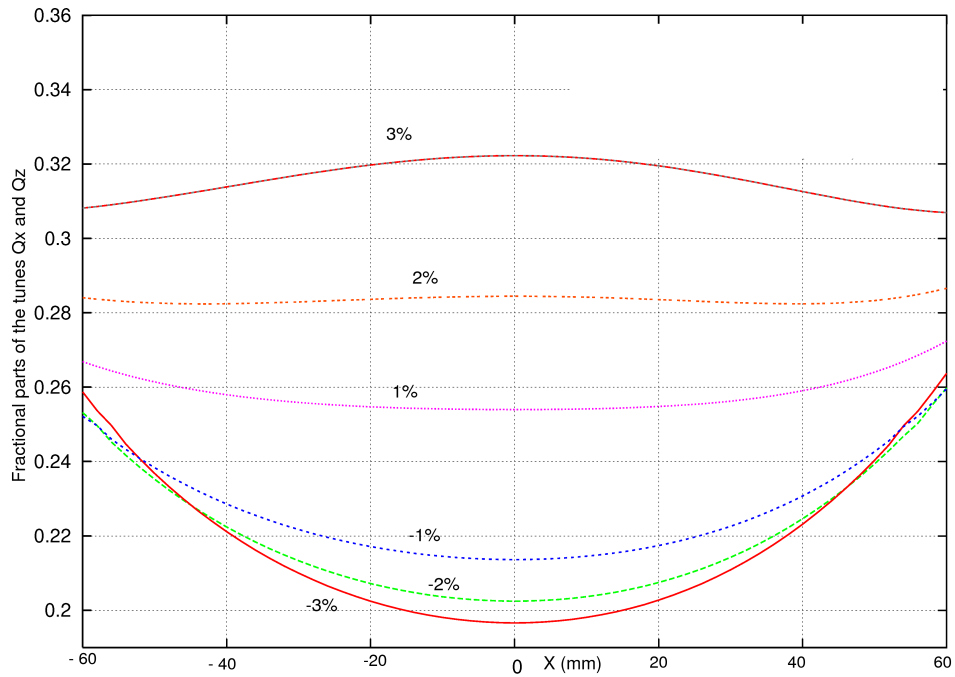


Figure 4.9: Horizontal tune shifts with amplitude for the off-momentum particles from -3% to 3% as indicated on the graph.

It is obvious from the graph that the indicated particles doesn't cross any dangerous resonance during their excursions except the -3% off-momentum particle which crosses the fifth order resonance at $X = \pm 15\text{mm}$.

It deserve to be mentioned here that this amplitude will be already outside the physical aperture (-27.5mm) if we remembered that the chromatic closed orbit of the -3% off-momentum particle will be at least at $X = -17\text{mm}$. So, the total oscillation amplitude will be at least -32mm .

Tracking the extreme off-momentum particles of $\Delta p/p = 3\%$ and -3% , as an example, around their closed orbits in the horizontal and vertical phase spaces shows the stability of these particles inside the vacuum chamber. This is shown by figures (4.10), (4.11), (4.12) and (4.13) respectively.

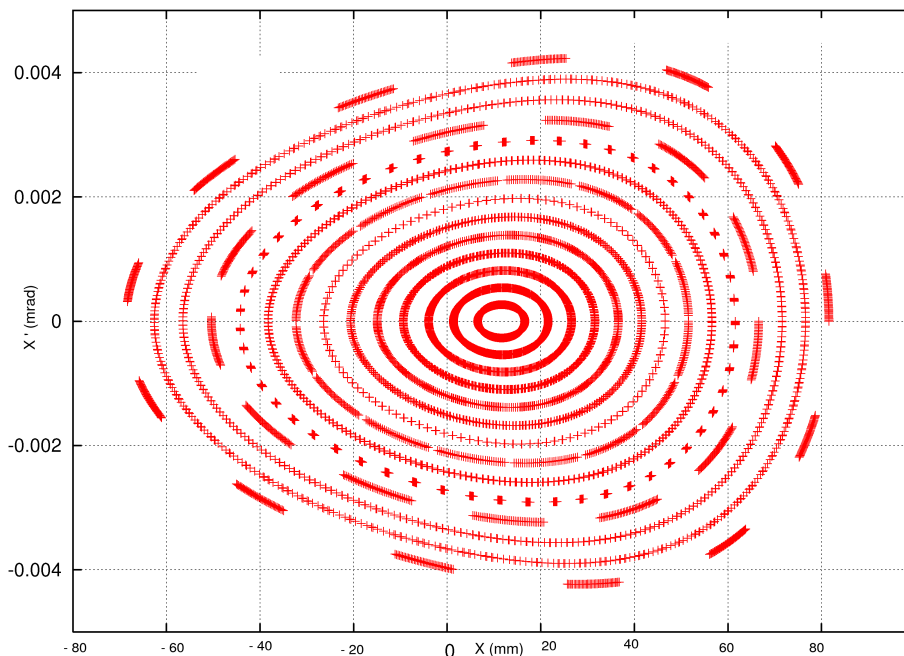


Figure 4.10: Tracking of the 3% off-momentum particle, around its chromatic orbit, in the horizontal phase space.

The high order resonances starting at $x = 50\text{mm}$ in figure (4.9), $x = 25\text{mm}$ are not dangerous since they are followed by stable regions. On the other hand, they are out of the physical aperture.

The figure (4.12) shows the 5th order resonance crossed by the -3% off-momentum particle at $X = \pm 15\text{mm}$. In addition to that it is outside the physical aperture, this resonance seems to be not dangerous because it is followed by a stable orbits so it doesn't cause the particle to be lost. This can be certified by the dynamic aperture graphs.

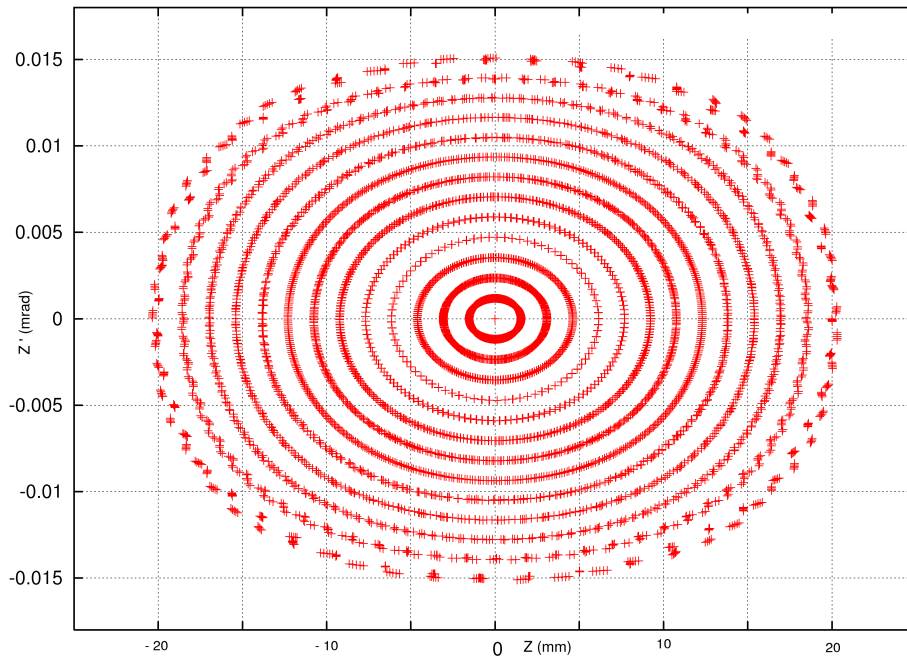


Figure 4.11: Tracking of the 3% off-momentum particle in the vertical phase space.

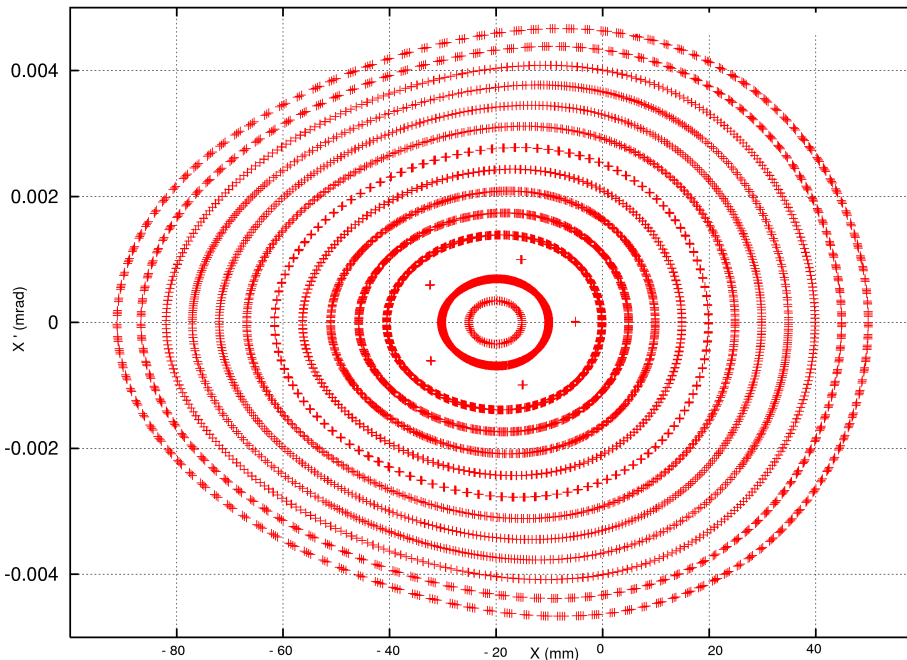


Figure 4.12: Tracking of the -3% off-momentum particle in the horizontal phase space.

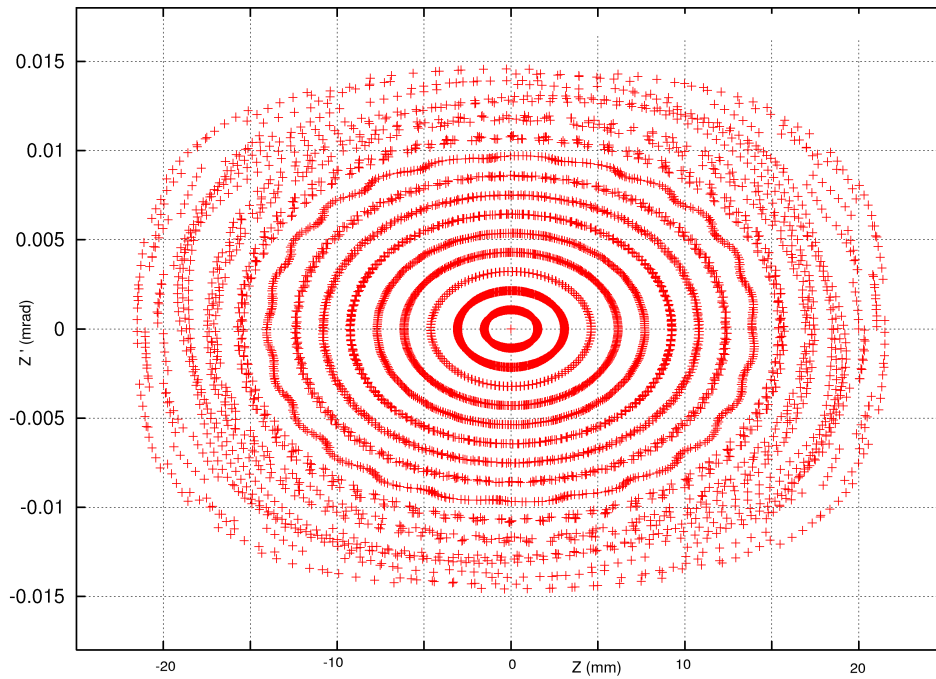


Figure 4.13: Tracking of the -3% off-momentum particle in the vertical phase space.

Dynamic apertures of the 3% and -3% off-momentum particles reveals more the stability levels of these particles. This can be seen by figures (4.14) and (4.15).

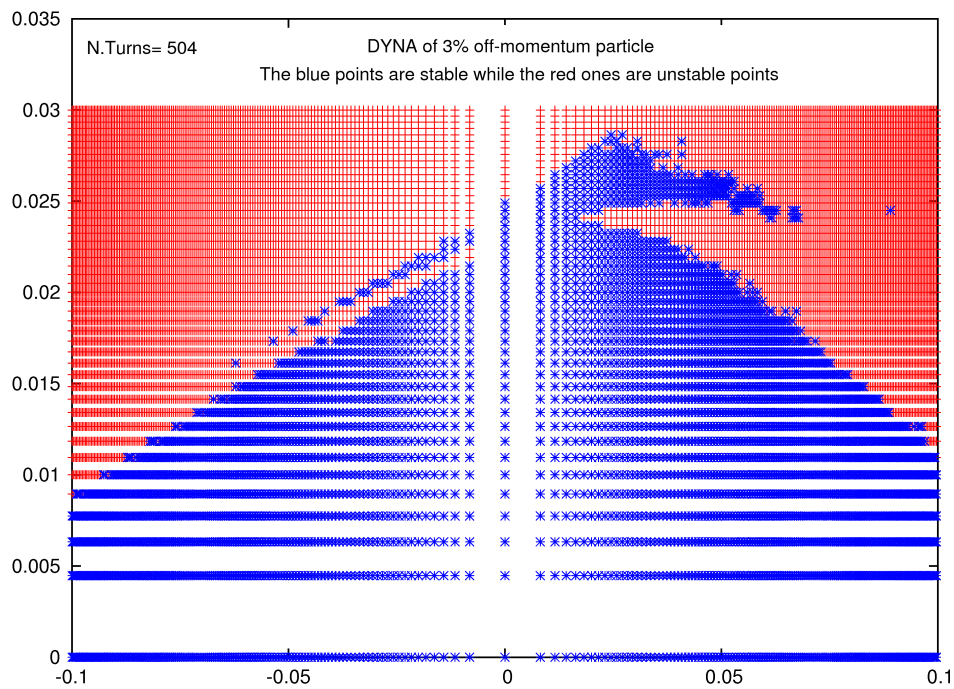


Figure 4.14

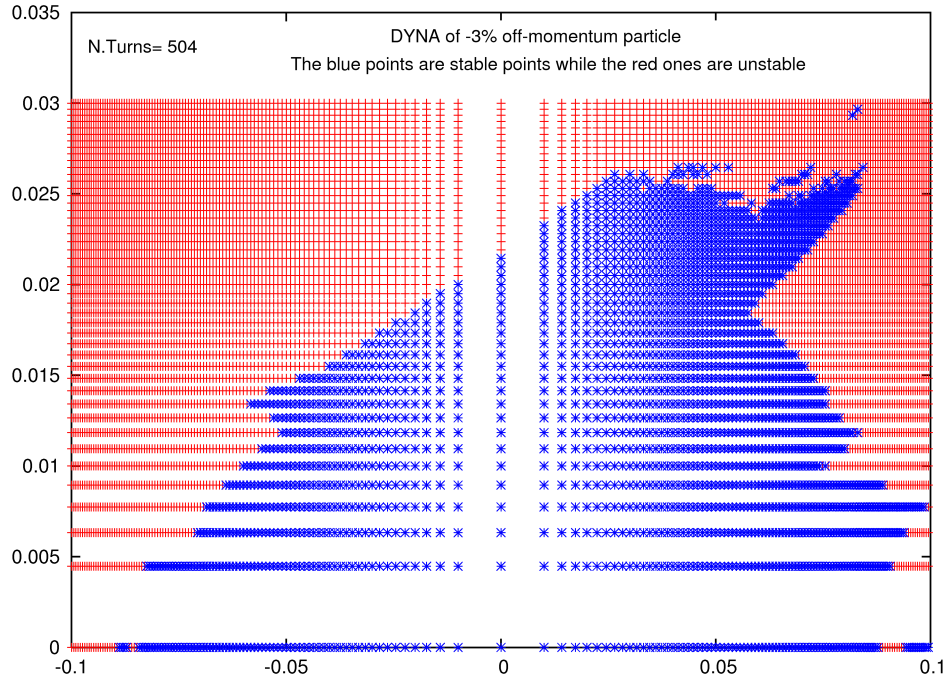


Figure 4.15

4.3 The Machine Acceptance

In SESAME IV ideal case, the machine physical acceptance is again limited by the vacuum chamber acceptance as shown by figure(4.16). The calculations have been done at the beginning of the ring where the septum will be. One can hope that the dynamic acceptance will be still larger than the chamber one under the multi-pole effect in case if the magnetic elements were well manufactured.

On the condition that the septum will be at $x = -27.5\text{mm}$, the horizontal acceptance (for the on-momentum particle) = $4.85 \times 10^{-5} \text{ m.rad}$. Vertically, it will be limited by the in-vacuum undulator half-gap (3 mm), which makes the vertical acceptance to be $3.73 \times 10^{-6} \text{ m.rad}$.

Since the dynamic acceptance is much larger than the chamber one, as shown in figure (4.16), we are again limited transversely by the vacuum chamber (specifically by the septum magnet).

Figure (4.17) shows the change in the transverse energy acceptance along one super period of SESAME IV ring. The positive energy acceptance ($\epsilon_{t,acc} > 0$) is shown in blue while the negative one ($\epsilon_{t,acc} < 0$) is shown in red. It can be seen that the minimum energy acceptance is at the middle of the bending magnet and it is about 1.95 % in the positive side of the chamber and about -2.1 % in the negative side of the chamber.

But since the RF energy acceptance of SESAME will be around 1.46 % at the beginning, the machine energy acceptance will be limited only by the RF one.

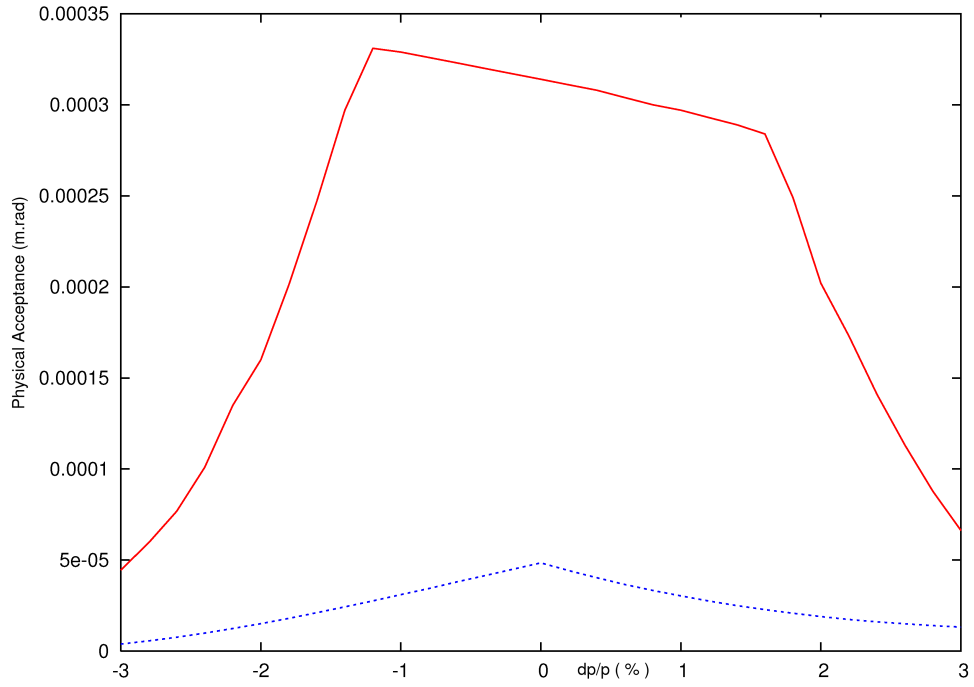


Figure 4.16: The ideal dynamic acceptance (in red) and the physical one determined by the septum magnet (in blue) as a function of δ .

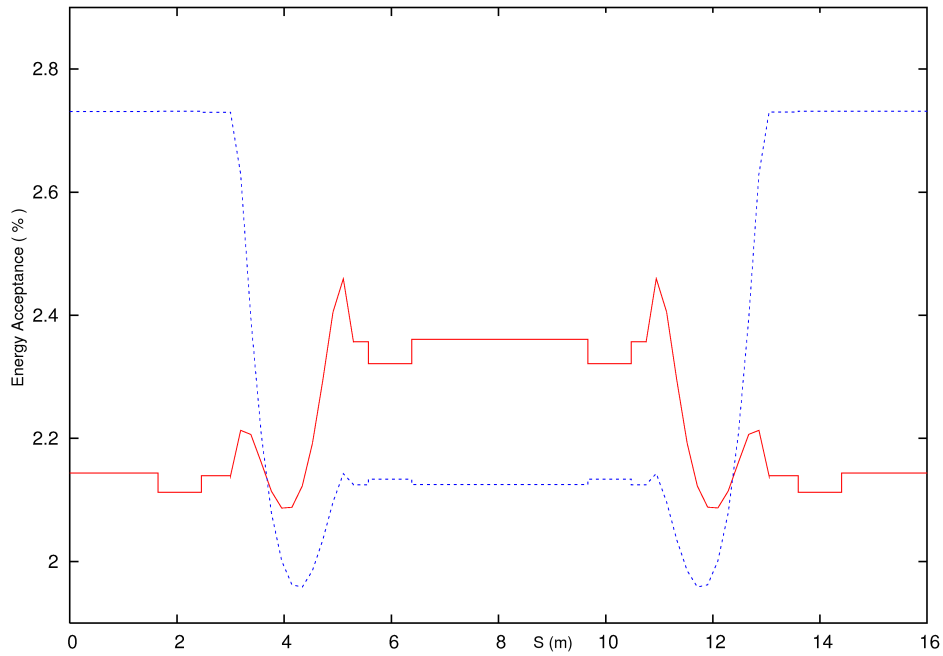


Figure 4.17: The absolute energy acceptance change through the super period of SESAME IV ring. The positive energy acceptance is in blue and the negative one is in red.

4.3 Effect of Insertion Devices on SESAME Optics

The optimum optics for installation of some ID configuration can be found using the same manner mentioned in chapter 4, section 4.4.

4.3.1 The Compensation for the Undesirable Effects

The main feature of the compensation scheme for SESAME IV lattice is that it is local in case of installing different types and numbers of IDs. This will increase the number of the needed power supplies due to the increase in the number of quadrupole families.

Also, to have a good level of compensation, two families of quadrupoles (one focusing and another defocusing) are needed to be around the ID in the same straight section. It has been found that one family doesn't work.

Due to the fact that SESAME IV lattice has two quadrupole families in one ID section and one family in the other one, and due to the fact that the need for good compensation scheme depends on the strength of the ID, it has been seen to put the wigglers (strong ID) in the section of two quadrupole families and the undulators (weak ID) in the section of one quadrupole family.

The Case of 8 Similar Wigglers: again there was no beta beating because of the convenience between the number of wigglers and the storage ring symmetry. The resulted vertical tune shift has been compensated *globally* using the two families of quadrupole.

The wiggler that has been used was an ideal one with $B = 3\text{T}$ and $L = 2.4\text{m}$. Figure (4.18) shows the optics with 8 wigglers after tune compensation.

The dynamic aperture was again positively affected by the wiggler magnetic fields which made no need to compensate for the non linear effects.

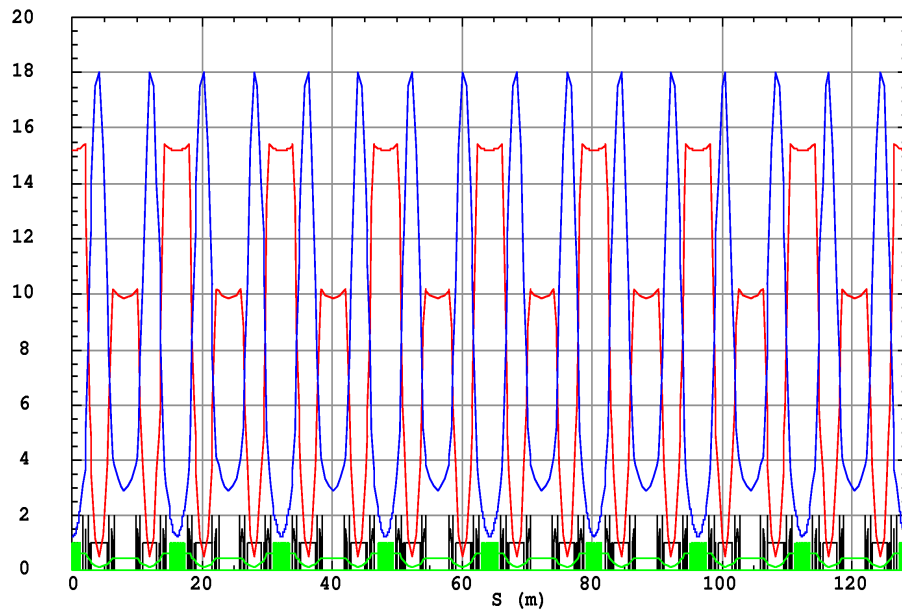


Figure 4.18: The optics with 8 wigglers of $B = 3\text{T}$ and $L = 2.4\text{m}$ after tune compensation. The total ring is shown.

The Cases of Less than 8 Wigglers of Different Types:

In case of different configurations of different wigglers, the compensation of tune shifts and beta beating is done *locally*. The two families of quadrupoles close to each different wiggler are put in a new family. This increased the number of variables used in correction process. A scheme of alpha correction (to ask that α_x and α_z be zero in some symmetrical points in the ring) and beta value correction has been used.

Figures (4.19, 4.20 and 4.21) show the optics after compensating the tune shift and beta beating in case of one, two and three wiggler configurations respectively.

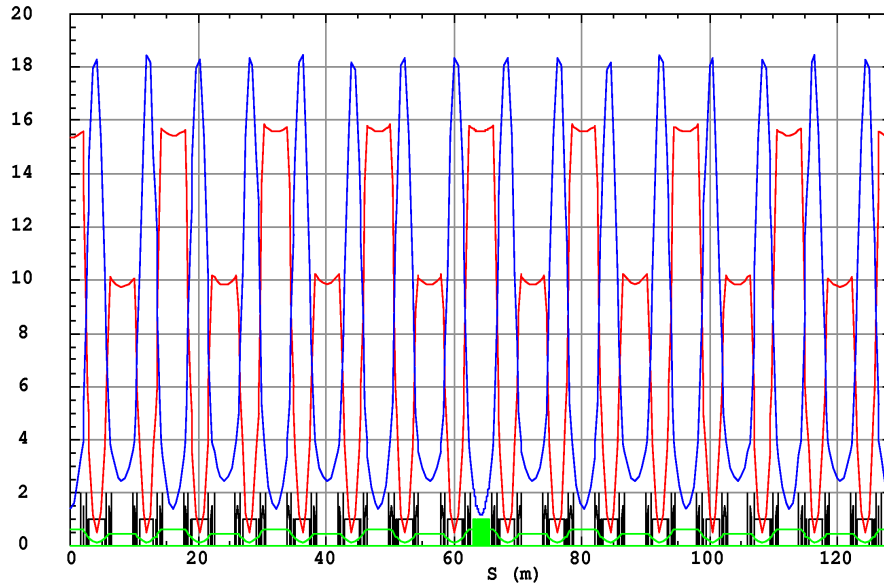


Fig. 4.19: The optics with 1 wiggler of $B=3T$ and $L=2.4m$ after compensation.

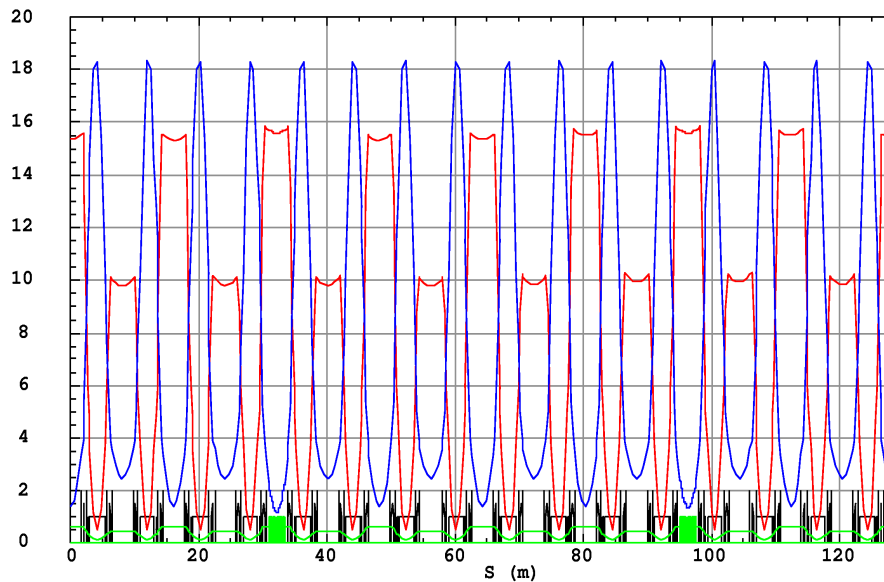


Fig. 4.20: The optics with 2 wigglers of $(B= 3T, L= 2.4m)$ and $(B=2T, L=2.4)$ after compensation.

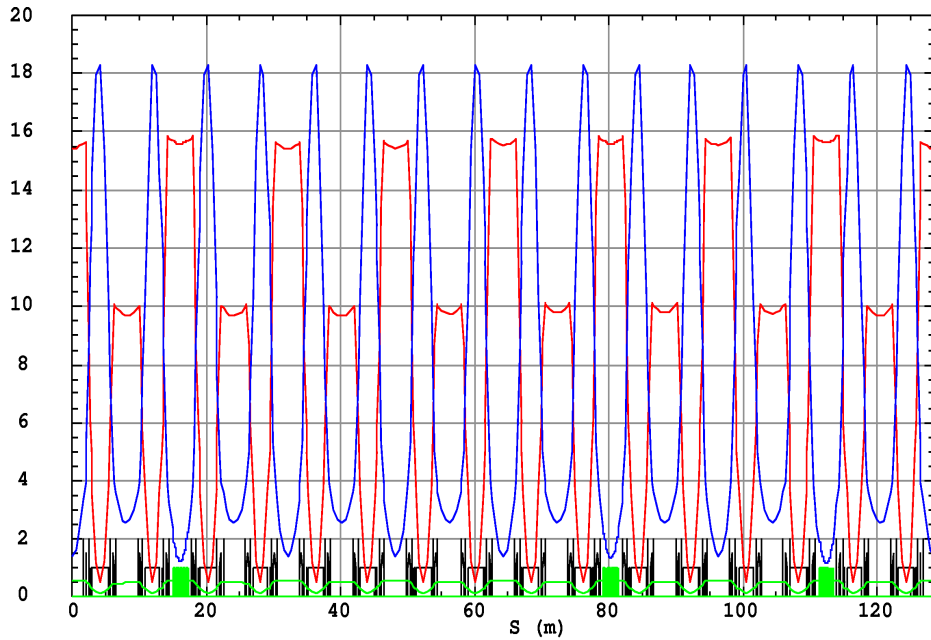


Fig. 4.21: The optics with 3 wigglers of ($B= 2.5T, L= 2.4m$), ($B=1.5T, L= 2.4m$) and ($B= 3.5T, L=2m$) after compensation.

The dynamic apertures were reduced in these cases, but they are still larger than the needed physical aperture as shown in figures (4.22 and 4.23) for a particle tracked over 1000 turns. However they can be enhanced by nonlinear optimisation using the four families of sextupoles.

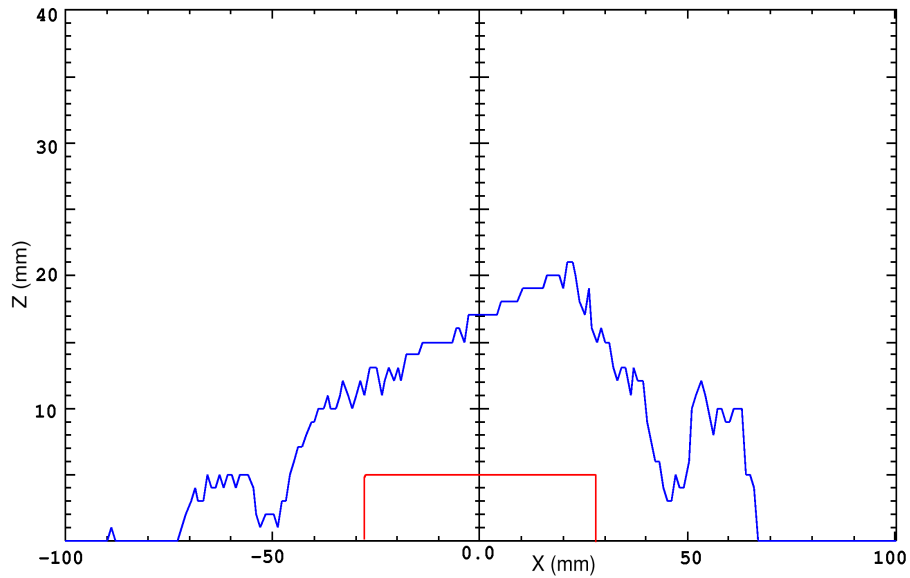


Figure 4.22: The dynamic aperture with 1 wigglers of $B= 3T$ and $L= 2.4m$ after the total compensation.

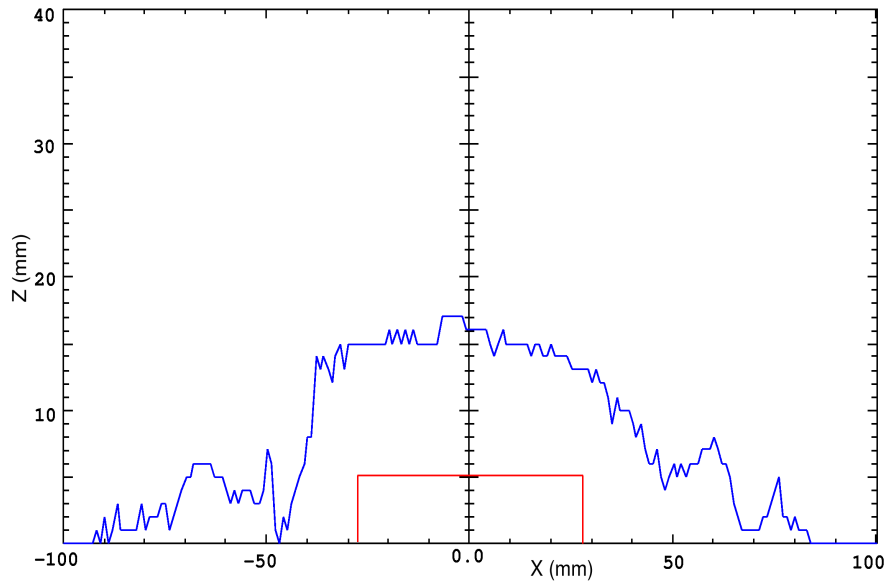


Figure 4.23: The dynamic aperture with 2 wigglers of ($B= 3T$, $L= 2.4m$) and ($B= 2T$, $L=2.4m$) after the total compensation.

4.4 Closed Orbit Distortion and Correction

Introducing the same statistical errors of SESAME III in SESAME IV, the expected closed orbit distortion is similar to the previous case with less sensitivity of the vertical plane to errors due to the less gradient in the bending magnets in SESAME IV lattice.

The scheme of the closed orbit correction here is also similar to the previous case of SESAME III.

4.5 Specifications of the Magnets

4.5.1 The Bending Magnets

All these elements in the storage ring have the same parameters, so they are in one family. Their parameters are displayed by table (4.3):

Table 4.3: Magnetic parameters of the BMs.

Parameter	Unit	Value
Magnetic Length	m	2.3
Bending angle	radian	.3927
Bending radius	m	5.852
Magnetic field gradient	T/m	-2.377

4.5.2 The Quadrupole Magnets

These elements are divided into 3 families; 2 horizontally focusing and 1 vertically focusing families. Their parameters are shown in table (4.4):

Table 4.4: Magnetic parameters of the quadrupoles.

Family	Q1	Q2	Q3
Magnetic Length (m)	.26	0.11	0.26
Magnetic field gradient (T/m)	18.8	-17.2	18.48

4.5.3 The Sextupole Magnets

These elements are divided into 4 families, each family has the same parameters as shown in table (4.5). The sextupole strength (\mathbf{m}) is defined by $\mathbf{m}(\text{m}^{-3}) = (1/2B\rho)\partial^2 B_z/\partial x^2$.

Table 4.5: Magnetic parameters of the sextupoles.

Family	S1	S2	S3	S4
Magnetic Length (m)	0.14	0.14	0.14	0.14
Magnetic Strength (m^{-3})	5.972	-8.26	-17.02	12.29

4.5.4 The Corrector Magnets

These elements will be as coils inside the sextupoles having the same length of the sextupoles. There will be two types of correctors to correct the closed orbit: horizontal and vertical ones to correct the horizontal and vertical closed orbit distortion, respectively. Table (4.6) shows their parameters.

Table 4.6: Magnetic parameters of the corrector magnets.

Type of Corrector	Horizontal	Vertical
Magnetic Length (m)	0.14	0.14
Maximum Kick (radian)	$1.115 \cdot 10^{-4}$	$7.113 \cdot 10^{-5}$

4.6 The Beam Lifetime

4.6.1 The Gas Scattering Lifetime

4.6.1.1 Elastic Nucleus-Scattering Lifetime (τ_{coul}):

The minimum vertical half-aperture will be, at the in-vacuum undulator, of 3mm. This made the minimum vertical acceptance to be there:

- $(A_z^2/\beta_z) = (0.003)^2/2.41 = 3.73 \times 10^{-6}$ m.rad.

On the condition that the septum will be at $x = 27.5$ mm, it will limit the horizontal acceptance which will be:

- $(A_x^2/\beta_x) = (0.0275)^2/15.6 = 4.848 \times 10^{-5}$ m.rad.

With $\langle\beta_x\rangle = 8.4715$ m and $\langle\beta_z\rangle = 7.805$ m in the storage ring, the nucleus-Coulomb scattering at $P = 2$ nTorr is expected to be:

$$\tau_{\text{Coul}} = 31.33 \text{ hours}$$

While at $P = 1$ nTorr, it will be:

$$\tau_{\text{Coul}} = 62.66 \text{ hours}$$

4.6.1.2 Elastic Shell Electron-Scattering Lifetime ($\tau_{\text{coul}}(e)$):

The machine energy acceptance will be limited by the RF one which is 1.46% (without Insertion Devices). This lifetime at $P = 2$ nTorr is expected to be:

$$\tau_{\text{Coul}}(e) = 1479.98 \text{ hours}$$

While at $P = 1$ nTorr, it will be:

$$\tau_{\text{Coul}}(e) = 2959.96 \text{ hours}$$

Due to its large value, the effect of this lifetime component on limiting the total beam lifetime will be negligible.

4.6.1.3 Inelastic Nucleus-Scattering Lifetime (τ_{brem}):

This lifetime is proportional to the minimum energy acceptance which will be the RF one at the beginning.

With the RF acceptance of 1.46%, at $P=2 \text{ nTorr}$ the lifetime is expected to be:

$$\tau_{\text{Brem}} = 29.1 \text{ hours}$$

while at $P=1 \text{ nTorr}$, it will be:

$$\tau_{\text{Brem}} = 58.2 \text{ hours}$$

4.6.1.4 Inelastic Shell Electron-Scattering Lifetime ($\tau_{\text{brem}}(e)$):

Having an RF energy acceptance of 1.46% and at $P=2 \text{ nTorr}$, this lifetime is expected to be:

$$\tau_{\text{Brem}}(e) = 68.1 \text{ hours}$$

while at $P=1 \text{ nTorr}$, it will be:

$$\tau_{\text{Brem}}(e) = 136.16 \text{ hours}$$

4.6.1.5 The Total Gas Scattering Lifetime

So, the total gas scattering lifetime (τ_g) is calculated as:

$$1/\tau_g = 1/\tau_{\text{Coul}} + 1/\tau_{\text{Coul}}(e) + 1/\tau_{\text{Brem}} + 1/\tau_{\text{Brem}}(e) \quad (4.11)$$

which means that τ_g at $P=2 \text{ nTorr}$ is calculated to be:

$$\tau_g = 12.25 \text{ hours}$$

while at $P=1 \text{ nTorr}$, it will be:

$$\tau_g = 24.5 \text{ hours}$$

4.6.2 Touschek Scattering Lifetime

The machine acceptance will be again limited by the RF one (1.46%).

The Touschek lifetime has been calculated for the following constant conditions:

- The maximum momentum deviation $\Delta P/P = \pm 1.6\%$
- The RF energy acceptance = 1.46%.
- The coupling = 1%
- The natural bunch length = $3.71257 \times 10^{-11} \text{ s}$
- The vacuum chamber half-dimensions are 15mm vertically but 3mm at the in-vacuum undulator and 35mm horizontally but 27.5mm at the septum.
- On the condition that a 70% of the storage ring will be filled with current of 400mA, the (beam current/ bunch) (I_b) will be: $I_b = 2.67 \text{ mA}$.

According to the above conditions, Touschek lifetime τ_{Tous} has been calculated to be:

$$\tau_{\text{Tous}} = 74.3 \text{ h.}$$

It should be noted that the effect of I_b value on the bunch length was not taken into account.

4.6.3 The Total Beam Lifetime

According to the above calculations, the total beam lifetime is expected to be, at $P=2n\text{Torr}$: $\tau = 10.5$ h, while at $P=1n\text{Torr}$: $\tau = 18.4$ h.

4.7 The Effect of High Order Multipoles on SESAME IV Beam Dynamics

The above calculations have been done for an ideal machine, which will not be the case in the normal life. In practise the magnetic elements will not be ideal since the finite magnetic poles will result in natural higher order systematic multipoles. On the other hand, the manufacturing errors in the same element produces another random multipoles.

These unwanted multipoles result in magnetic field error which has a destructive effect on the beam dynamics. The dynamic aperture is minimised due to the change in the tune shift with amplitude together with some resonances excited by the high order multipoles. The momentum aperture could be affected due to the new tune shift with energy deviation.

The investigation on the lattice sensitivity to these multipole errors is a crucial task that should be done and the tolerable magnetic field error should be determined.

The tolerance of SESAME IV lattice to the effect of high order multipoles in the dipoles, quadrupoles and sextupoles has been investigated. To have a real feeling about the lattice tolerance, the measured and simulated error multipoles in the elements of several machines (SPEARIII, ASP, ANKA, SLS and BESYII) have been used in SESAME lattice.

The effect of the high order multipoles on the beam dynamics will be represented by the behaviour of the on-momentum and off-momentum dynamic apertures because any impact of the field error on the tune shift with amplitude or with energy deviation will be translated to distorted and minimized dynamic apertures.

4.7.1 Dipoles including Multipoles

The total magnetic field expansion is given by the following polygon:

$$B = B_1 + B_2 * x + B_3 * x^2 + B_4 * x^3 + B_5 * x^4 + B_6 * x^5 + B_7 * x^6 + B_8 * x^7 + B_9 * x^8 + B_{10} * x^9$$

where B_1 is the original magnetic flux and B_2, B_3, \dots are the gradients (multipole coefficients) of the different multipole components. The magnetic field error produced by the high order multipoles has been calculated at $x = 22\text{mm}$ from the nominal orbit. The tolerable values of the different multipole coefficients were :

$$B_3 = 0.3 \text{ T/m}^2 \quad (6\text{-pole})$$

$$B_4 = 10.0 \text{ T/m}^3 \quad (8\text{-pole})$$

$$B_5 = 320.0 \text{ T/m}^4 \quad (10\text{-pole})$$

$$B_6 = 1.2 * 10^4 \text{ T/m}^5 \quad (12\text{-pole})$$

$$B_7 = 3.6 * 10^5 \text{ T/m}^6 \quad (14\text{-pole})$$

$$B_8 = 1.2 * 10^7 \text{ T/m}^7 \quad (16\text{-pole})$$

$$B_9 = 4.0 * 10^8 \text{ T/m}^8 \quad (18\text{-pole})$$

$$B_{10} = 1.3 * 10^{10} \text{ T/m}^9 \quad (20\text{-pole})$$

The resulted magnetic field errors with x in the gradient bending magnet are given in figure (4.24).

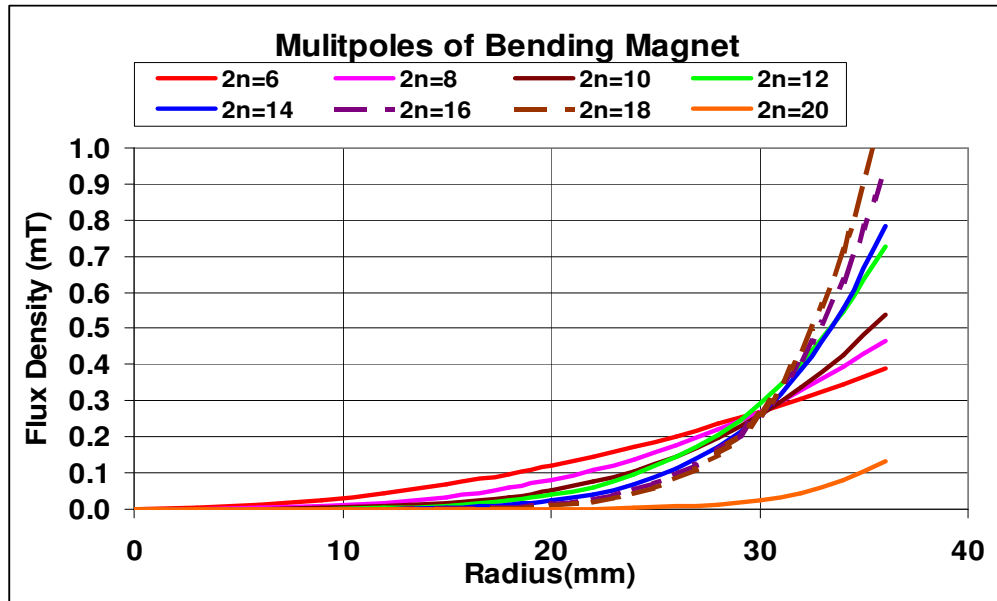


Figure 4.24 : The magnetic field error with x due to high order multipoles in SESAME bending magnet.

The on-momentum and off-momentum dynamic apertures with these multipoles are shown by figure (4.25):

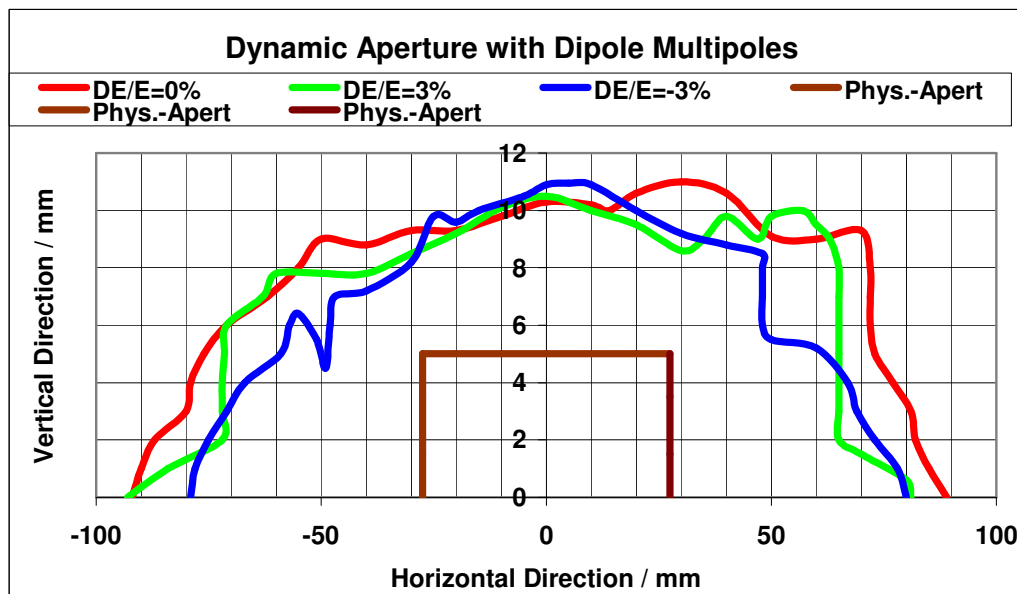


Figure 4.26: the on-momentum and off-momentum (3% and -3%) dynamic apertures under the effect of the high order multipoles in the dipole.

4.7.2 Quadrupoles including Multipoles

The multipole effect is calculated at $x = 35\text{mm}$ in the quadrupole. After an investigation on the effect of these multipoles on the beam dynamics, the tolerable multipole coefficients up to 28-pole component were calculated.

Due to the different quadrupole strengths, the multipole coefficients will be different for each quadrupole family. The maximum values of the multipole coefficients were:

- $B_3 = 0.29 \text{ T/m}^2$ (6-pole)
- $B_4 = 9.2 \text{ T/m}^3$ (8-pole)
- $B_5 = 2.86 \cdot 10^2 \text{ T/m}^4$ (10-pole)
- $B_6 = 1.8 \cdot 10^4 \text{ T/m}^5$ (12-pole)
- $B_7 = 2.8 \cdot 10^5 \text{ T/m}^6$ (14-pole)
- $B_8 = 8.7 \cdot 10^6 \text{ T/m}^7$ (16-pole)
- $B_9 = 2.7 \cdot 10^8 \text{ T/m}^8$ (18-pole)
- $B_{10} = 8.5 \cdot 10^9 \text{ T/m}^9$ (20-pole)
- $B_{11} = 2.7 \cdot 10^{11} \text{ T/m}^{10}$ (22-pole)
- $B_{12} = 8.4 \cdot 10^{12} \text{ T/m}^{11}$ (24-pole)
- $B_{13} = 2.6 \cdot 10^{14} \text{ T/m}^{12}$ (26-pole)
- $B_{14} = 5.3 \cdot 10^{15} \text{ T/m}^{13}$ (28-pole)

The magnetic field error with x due to these multipoles is shown by figure (4.27), while the total magnetic field deviation due to all the multipole component is shown by figure (4.28).

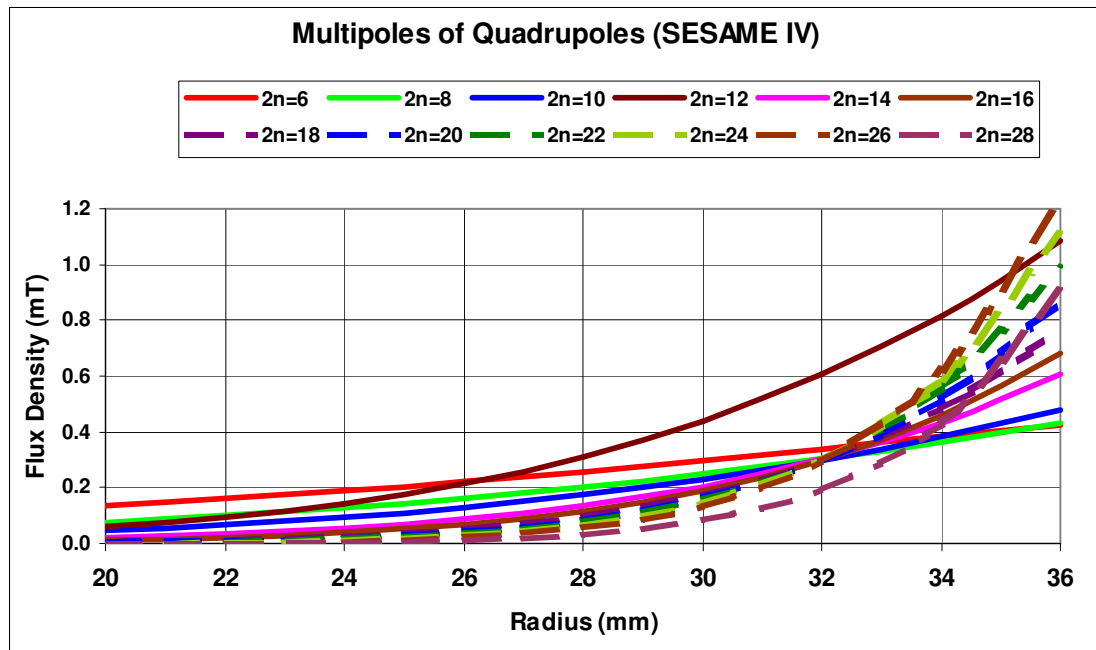


Figure 4.27 : The magnetic field error with x due to high order multipoles in SESAME quadrupole magnet.

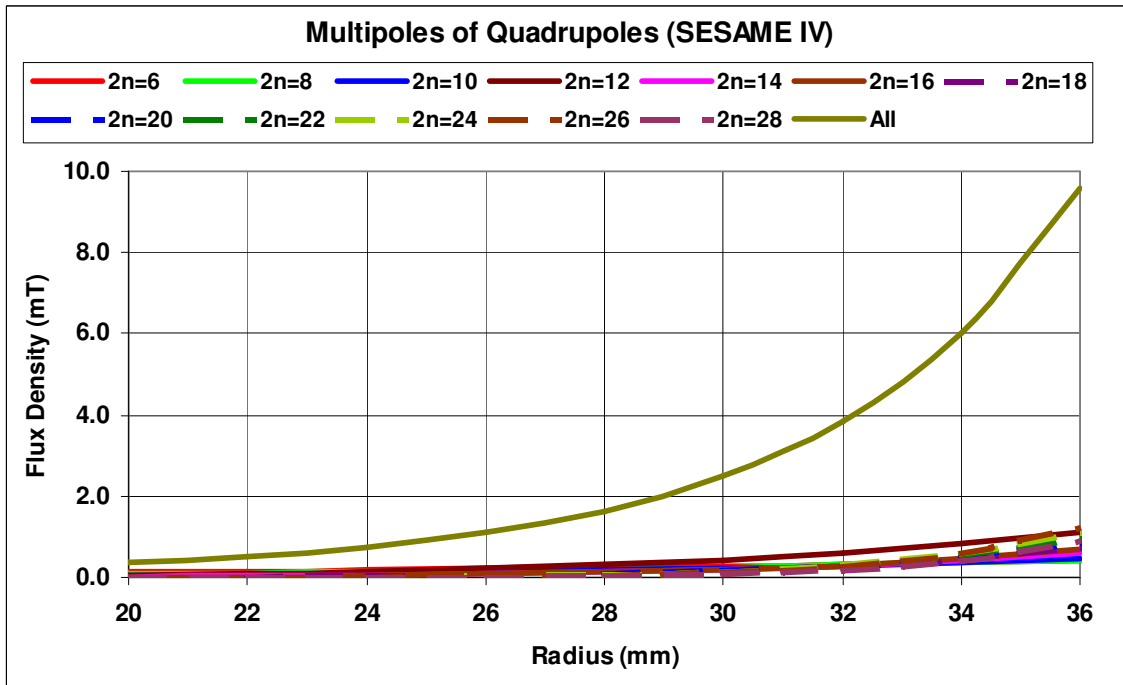


Figure 4.28 : The total field error together with the errors due to each multipole component in the quadrupole.

The effect of these multipoles on the on-momentum and off-momentum dynamic apertures appears in figure (4.29).

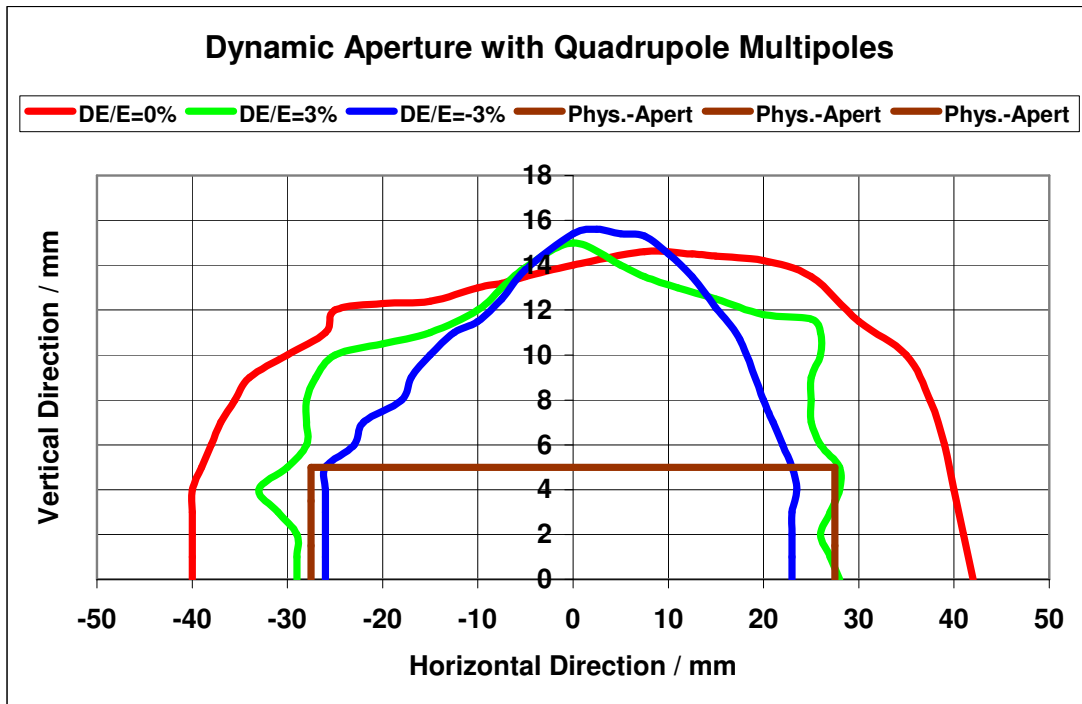


Figure 4.29: The effect of the quadrupole multipoles on the on-momentum and off-momentum dynamic apertures.

4.7.3 Sextupoles including Multipoles

The multipole effect has been calculated here also at $x = 35\text{mm}$. The systematic multipoles (18-pole, 30-pole and 42-pole) were the most effective ones, so a care should be taken about their optimisation. The maximum multipole coefficients tolerable by the lattice- up to 42-pole component- were:

$B_4 = 1.83 \text{ T/m}^3$	(8-pole)
$B_5 = 5.7 \cdot 10^1 \text{ T/m}^4$	(10-pole)
$B_6 = 9.0 \cdot 10^3 \text{ T/m}^5$	(12-pole)
$B_7 = 5.6 \cdot 10^4 \text{ T/m}^6$	(14-pole)
$B_8 = 1.8 \cdot 10^6 \text{ T/m}^7$	(16-pole)
$B_9 = 2.8 \cdot 10^9 \text{ T/m}^8$	(18-pole)
$B_{10} = 1.7 \cdot 10^9 \text{ T/m}^9$	(20-pole)
$B_{11} = 5.3 \cdot 10^{10} \text{ T/m}^{10}$	(22-pole)
$B_{12} = 1.7 \cdot 10^{12} \text{ T/m}^{11}$	(24-pole)
$B_{13} = 5.2 \cdot 10^{13} \text{ T/m}^{12}$	(26-pole)
$B_{14} = 1.6 \cdot 10^{15} \text{ T/m}^{13}$	(28-pole)
$B_{15} = -8.7 \cdot 10^{17} \text{ T/m}^{14}$	(30-pole)
$B_{16} = 1.6 \cdot 10^{18} \text{ T/m}^{15}$	(32-pole)
$B_{17} = 5.0 \cdot 10^{19} \text{ T/m}^{16}$	(34-pole)
$B_{18} = 1.6 \cdot 10^{21} \text{ T/m}^{17}$	(36-pole)
$B_{19} = 5.0 \cdot 10^{22} \text{ T/m}^{18}$	(38-pole)
$B_{20} = 1.5 \cdot 10^{24} \text{ T/m}^{19}$	(40-pole)
$B_{21} = 8.0 \cdot 10^{25} \text{ T/m}^{20}$	(42-pole)

The field error produced by each systematic multipole together with the total field error are shown by figure (4.30). The effect of these multipoles on the dynamic apertures is shown in figure (4.31).

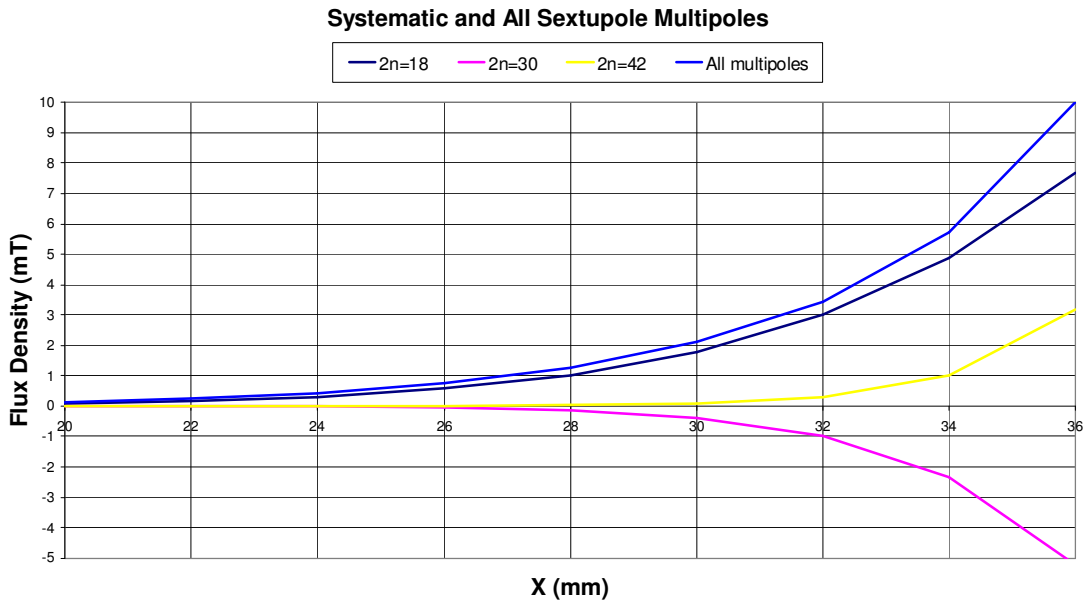


Figure 30: The field deviation due to the systematic multipoles.

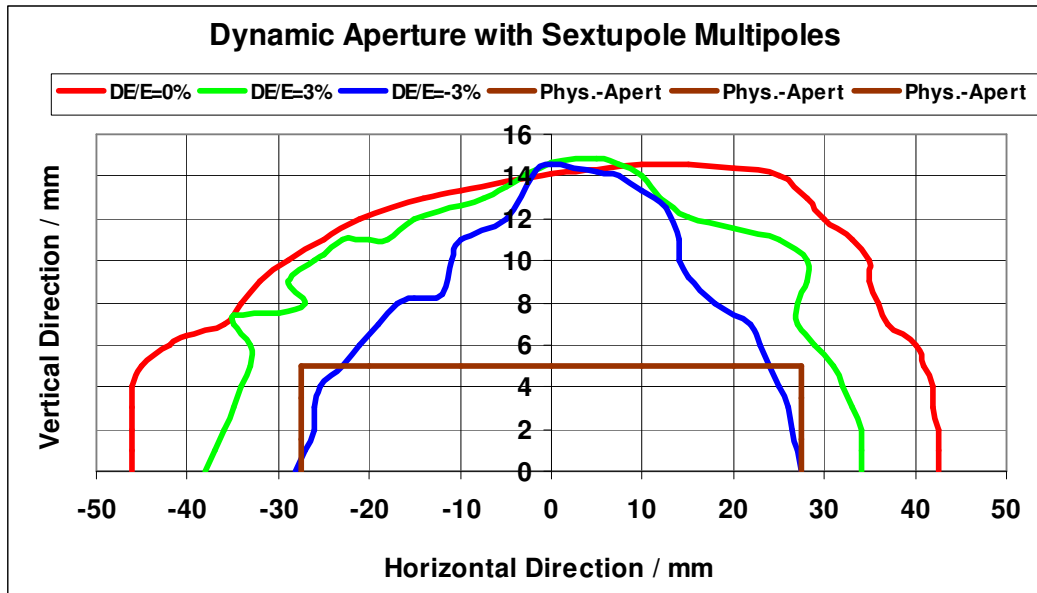


Figure 4.31: The effect of the sextupole multipole contents on SESAME IV dynamic apertures.

4.7.4 All Magnets including Multipoles

After studying the effect of multipole contents of each element alone, the total effect has been investigated by introducing the multipoles of all the elements to SESAME IV lattice. This is more realistic case. The total effect on the dynamic apertures is shown in figure 4.32.

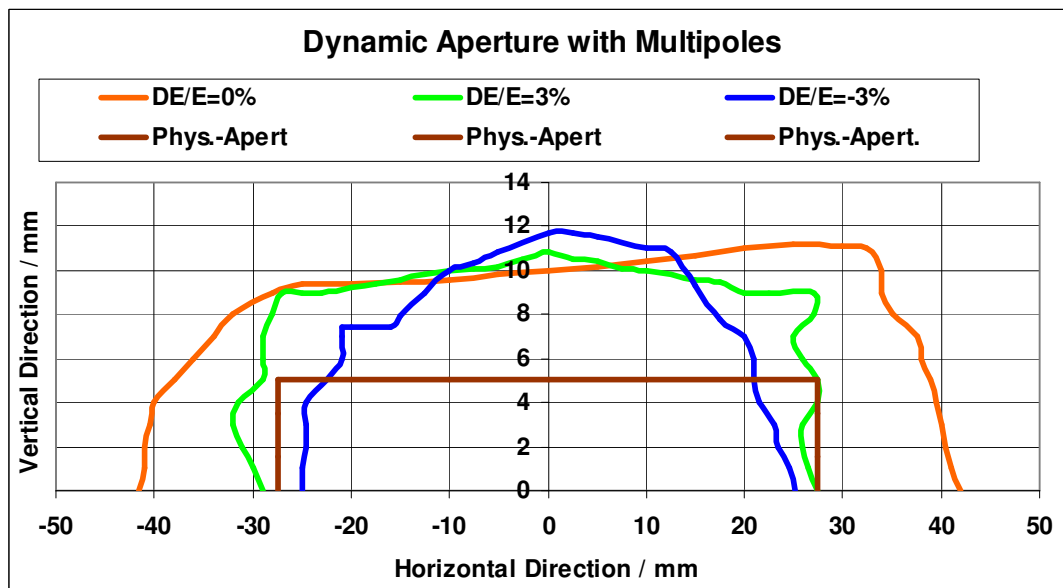


Figure 4.32: The effect of all the magnetic multipoles on the dynamic apertures.

It should be taken into account that the -3% off-momentum particle has an allowed aperture of about 11mm from its chromatic closed orbit. According to this fact, the shown dynamic aperture of this particle is larger than the physical aperture in all the above cases.

The results of the multipole effect investigation show high beam stability and a lattice of a good tolerance to the real case errors.

References

- [1] The first white book and its references.